Reduction of pulsed particle load with dynamic pressure induced by transient recycled neutral flux

Yuki Hayashi[1,2*], Hirohiko Tanaka[3], Noriyasu Ohno[3], Shin Kajita[4], Thomas Morgan[5], Hennie van der Meiden[5], John Scholten[5], Jordy Vernimmen[5], Hiroki Natsume[3], Keiji Sawada[6], Shota Masuda[6]

[1]*National Institute for Fusion Science, National Institutes of Natural Sciences, Toki 509-5292, Japan*

[2]*The Graduate University for Advanced Studies, SOKENDAI, Toki 509-5292, Japan*

[3]*Graduate School of Engineering, Nagoya University, Nagoya 464-8603, Japan*

[4]*Graduate School of Frontier Sciences, The University of Tokyo, Kashiwa 277-8561, Japan*

[5]*DIFFER - Dutch Institute for Fundamental Energy Research, De Zaale 20, AJ Eindhoven 5612, the Netherlands*

[6]*Institute of Engineering, Shinshu University, Nagano 380-8553, Japan*

Abstract

From pulsed plasma experiments focusing on neutral pressure dependence, the impacts of a transition from a low to a high recycling target on the particle load were investigated and discussed in the linear plasma device, Magnum-PSI. Time traces of the target ion flux were mitigated in high neutral pressure cases because of a plasma-neutral interaction. On the other hand, in low neutral-pressure cases, the target ion flux indicated partial suppression in the last part of the pulse. The Langmuir probe, located 200 mm upstream from the target plate, did not exhibit such a suppression. Pulse suppression can be expected from the localized interaction between recycled neutral flux and pulsed plasma in front of the target. The mean-free paths of recycled neutral particles regarding the charge exchange with pulse ions and elastic scattering with background neutral particles were compared. Modeling using a fluid code coupled with a neutral transport code was performed, and it was concluded that dynamic pressure induced by the transient recycled neutral flux caused sufficient momentum loss to stagnate the pulsed plasma toward the target plate.

Keywords: Pulse plasma, Plasma detachment, Recycling, Langmuir probe, Magnum-PSI

[*]Author to whom correspondence should be addressed: hayashi.yuki@nifs.ac.jp

1. Introduction

Edge localized modes (ELMs) are a significant concern in ITER and conventional tokamaks operating in H-mode [1, 2]. ELMs collapse the pedestal and enhance heat flux across the separatrix, resulting in transient particle and heat transports from the scrape-off layer (SOL) to the divertor region along the magnetic-field line. Such transient heat loads, in addition to a steady-state heat load, must be handled in the SOL and divertor regions to increase the lifetime of divertor plates. A detached divertor provides a means of reducing steady-state heat loads via the plasma detachment phenomenon [3, 4]. A plasma operation scenario for ITER and future fusion devices is the H-mode accompanied by ELMs compatible with the detached divertor [5, 6]. On the other hand, the transition from a low to a high recycling divertor in association with an ELM event, has been represented as an important process [7]. After the ELM, instantaneous neutrals recycling from the divertor reach the main chamber by diffusion and change the upstream density profile in the SOL. The time evolutions of the D_α photon flux and ion particle flux into the divertor plates indicate the impact of the recycled neutral flux on the ionization process in ASDEX-U [7, 8] and JET [9]. A transient enhancement of the recycled neutral flux owing to the ELM is also expected in a detached plasma condition by the re-attachment process. Such an ELM-induced dynamic plasma-neutral interaction should be revealed to understand the after-ELM physics in front of the divertor plates.

Fundamental studies on the transition from a low to a high recycling regime and the enhancement of neutral flux from the divertor plates require specialized laboratory experiments. Combined experiments with steady-state detached plasma and heat pulses generated by radio frequency (RF) heating and modulated DC discharge power were performed in the linear plasma device NAGDIS-II [10, 11]. Rydberg atoms and/or neutral particles were ionized, by accelerated energetic electrons, resulting in the enhancement of the particle flux to the target plate. However, in future fusion devices such as ITER, ELMs will have extremely high ion densities and thus deliver large pulsed-ion particle fluxes to the target. It is necessary to investigate the interactions between the detached divertor and high-density pulsed plasma. Such experiments are realized in the linear plasma device Magnum-PSI because of its high performance for steady-state plasma generation with a particle flux of 10^{23}–10^{25} $m^{-2}s^{-1}$ and high-density pulsed plasma production [12, 13]. The density dependence of the pulsed heat load was studied in Magnum-PSI [14], which indicated the saturation of the peak heat load into the target in a high-density regime. Localized enhancement of the ionization and charge exchange (CX) processes was implied to constitute the energy-loss mechanism.

However, the dependence on neutral particle behavior such as neutral pressure has not been explored in detail. Furthermore, to investigate the interaction between pulsed plasma and transient recycling neutral particles, the measurement of particle flux, which is an indicator of recycling, is important, as well as heat flux. The present study elucidates the impacts of the transient enhancement of the recycling on the target ion flux into the detached divertor, after the pulsed plasma input, by focusing on neutral pressure dependence.

The next section describes the experimental conditions for Magnum-PSI in this study. The plasma parameters in the steady-state and transient phases during the pulse are presented in Section 3. Section 4 discusses the experimental observations, which provide a possible interpretation and derives conclusions. Finally, a summary is provided in Section 5.

2. Experimental setup

2.1. Plasma device

The linear plasma device Magnum-PSI [13, 15] was designed to address various complex plasma physics of the ITER divertor in a systematic investigation with high repeatability of plasma parameters, a flexible target setup, and good diagnostic access. Figure 1(a) schematically shows the experimental configuration used in the present study. Steady-state plasma is generated by a cascaded arc source which typically operates with an electrical current between 100 and 200 A from a DC power source (PS). A pulsed-plasma source designed to accommodate the transient pulses with high power was utilized to study the ELM simulation [16, 17]. The pulsed-plasma source consisted of a tungsten (W) cathode, six copper (Cu) cascaded plates, an anode, and a nozzle. The discharge channel diameter was 10 mm, which is larger than the standard trumpet source for most experiments without pulses, to minimize the impurity content in the plasma [16]. The anode and nozzle were grounded and made of a Cu-W alloy, coated with a W layer for protection from melting and impurity production. The plasma expanded into the vessel at the sound speed in the nozzle, owing to the pressure gradient from the discharge channel to the vessel. A large quantity of neutral gas was necessary to produce a high-flux plasma owing to its finite ionization efficiency. A differential pumping system removed most of the discharge gas from the source before reaching the target, enabling independent control of the target chamber pressure. The neutral pressure, p_n, in the target chamber was measured by the capacitance manometer (MKS Baratron®). The magnetic field, B, was provided by superconducting coils up to 2.5 T.

In the present study, the discharge current, I_{src}, and B were set to 120 A and 0.4 T, respectively. The discharge voltage, V_{src}, necessary to maintain I_{src} was ~82 V. The species used at the plasma source was helium (He) with a flow rate of 15 slm. The additional gas puff from

the target chamber was also He, with a flow rate of 0.0–6.9 slm, providing the p_n from 0.44 to 6.4 Pa. With an increase in p_n in the target chamber, a high degree of detachment was obtained, owing to the enhanced plasma-neutral interaction.

2.2. Pulse plasma generation

Figure 2 shows the discharge circuit. In parallel with the PS for steady-state plasma discharge, a capacitor bank (CB) system for the transient increase in the discharge power, P_{src}, was installed. The CB system consisted of 28 identical sections. Each section was composed of a capacitor with an electrostatic capacity of 150 μF, an inductor with an inductance of 160 μH, and an anti-reversal diode. After the capacitors were charged, the power supply to the capacitors was isolated, and the capacitor bank was connected to the plasma source. The stored energy could be then dissipated into the plasma by ohmic heating, leading to a transient increase in the electron density, n_e, and temperature, T_e. The capacitor voltage was 400 V for all results shown in the present study.

Figures 3(a)–(c) show the temporal evolutions of V_{src}, I_{src}, and P_{src} during the pulse. The trigger timing of the pulse corresponded to a time, t, of 0 ms. An analog-digital converter (NI PXI-5105) was utilized to acquire V_{src} reduced by the voltage divider and I_{src} measured by a current probe (Hioki 9667). During the pulse, the transient increase in V_{src} and I_{src} gave ~ 35 kW as the enhancement in the P_{src} curve, which was defined by the product of V_{src} and I_{src}. The dissipated energy of the pulse in the source plasma could be determined by integrating P_{src} over time during the pulse. Figure 3(d) shows the pulse energy dissipated in the plasma by the time-integrated process of the AC component of the P_{src}. The stored energy of the capacitor with a capacitor voltage of 400 V was theoretically calculated as 12 J. Figure 3(d) indicates that the practical pulse energy dissipated in the plasma was also ~ 12 J and was constant at various p_n conditions. Independent control of the plasma source enabled the demonstration of a constant pulse energy against the different p_n downstream.

2.3. Diagnostics

The steady-state and transient pulsed plasmas were measured using a Langmuir probe and target plate. Laser Thomson scattering (TS) measurements and optical emission spectroscopy (OES) were performed during the steady-state phase. Each of these diagnostics is explained in detail below:

A reciprocating Langmuir probe was mounted on the Magnum-PSI. The driving system was mainly composed of a probe head, an air cylinder, and a magnetic valve. The probe head consisted of four W electrodes with diameter of 0.5 mm and an exposed length of 0.5 mm

outside of an ceramic shaft. Two of the electrodes measured the ion saturation current, I_{sat}, with a bias voltage of -100 V and a floating potential, V_f, at the radial position, r, of ~ 0 mm. These signals were simultaneously obtained using an analog-digital converter (Yokogawa 720254). For the acquisition of I_{sat}, a shunt resistor of 100 Ω was used. To minimize the heat load, the probe head was extracted from the plasma column in every sequence, after acquiring the signal, during a pulse. Radial profile measurements were not performed using the probe. The probe head was inserted and extracted using an air cylinder driven by compressed air. The magnetic valve for controlling the compressed air was installed away from the device to protect it from the strong magnetic field and was remotely operated from the control room. Note that the probe driving system was also used in previous publications on Magnum-PSI [18, 19].

A target plate was installed 200 mm downstream of the probe position, as shown in figure 1. The plasma-facing material in the present experiments was mounted on one of the five target holders prepared for multiple targets [20]. The plasma-facing component was a circular W-plate with a diameter of 30 mm. A molybdenum (Mo) holder with a hole of 25 mm diameter held the W plate, indicating plasma exposure on the W, with a 25 mm diameter. The outer diameter of the Mo holder was 64 mm. Because every component of the target holder was electrically connected and negatively biased, the ion saturation current at the target, I_{target}, provided the total ion current of the plasma column. For I_{target} measurement, the target plate was maintained at – 60 V by the PS for the target plate. The target voltage for acquiring I_{target} was not negatively deep enough to avoid the arcing or sputtering at the target. An analog-digital converter (Yokogawa 720254) acquired the output signal of the current probe (Ion Physics CM-10-L). Here, the bias voltage of – 60 V was sufficient for the ion saturation even under the pulse condition, because V_f during the pulsed plasma was higher than – 60 V. The details of the V_f are explained in Section 3.2.

TS measurements with a high accuracy for n_e and T_e were performed at the probe position [21]. Radial profiles of n_e and T_e were obtained in the steady-state phase without a pulse. The OES was performed using a passive spectroscopy system (Avantes AvaSpec-2048) at the probe position. The line of sight of the optical fiber was aligned to pass through the center of the plasma column.

3. Experimental results

3.1. Plasma parameters in steady-state phase

Figure 4 shows the p_n dependences of the steady-state parameters without the pulse. Figures 4(a) and (b) show the He line emission intensities corresponding to the transitions from high-n excited levels (370.5 nm: 2^3P-7^3D and 355.4 nm: 2^3P-10^3D) and a low-n excited level

(471.3 nm: 2^3P-4^3S). Regarding the high-n emission, an increase up to p_n of 2–3 Pa is due to an enhancement of the electron-ion recombination (EIR) processes. A steep reduction in T_e at the plasma center measured by TS, as shown in figure 4(c), indicates the enhancement of EIR processes with an increase in p_n because a three-body recombination as an EIR process has a strong dependence on n_e and especially T_e [22, 23]. When the population of low-n states is determined by electrons excited from the ground state, the low-n emission should decrease with n_e and T_e except for p_n of 0.44 Pa. However, both low- and high-n emissions show similar tendencies, indicating that the transition from a highly excited level is dominant in determining the population of the 4^3S state in the present condition. The peak of n_e observed at 1.4 Pa indicates the rollover [24, 25]. Figures 4(d) and (e) show particle flux reductions with increasing p_n at both the Langmuir probe and target plate positions. These results indicate that EIR processes are strongly induced except for p_n of 0.44 Pa and the degree of detachment is enhanced by the increase in p_n.

Figure 5 shows the radial profiles of n_e and T_e at p_n values of 0.44, 3.0, and 6.4 Pa. Owing to the relatively low B in the present experiments, the plasma diameter, 20–30 mm, evaluated by the full width half maximum of n_e was larger than the typical width in Magnum-PSI [14]. However, even in the low B case, the diameter of the target plate is larger than the plasma diameter, and I_{target} represents the total ion flux into the target plate.

3.2. Transient response of plasma during the pulse

Figure 6 shows the time traces of P_{src}, I_{sat}, I_{target}, and V_f during the pulse at p_n of 3.0 Pa. Data acquisition during the pulse was performed four times under the same p_n conditions and all waveforms were averaged to ensure high reliability. Approximately 0.1 ms after the pulse was triggered, I_{sat} began to increase. Further I_{target} represented the attainment of the pulse at $t \sim$ 0.18 ms. Time delays that appeared in I_{sat} and I_{target} indicated that the pulsed plasma was transported along the magnetic field line with a finite flow velocity. The time lag between I_{sat} and I_{target} also indicated that pulse plasma transport could be detected even with a short length of 200 mm from the Langmuir probe and the target plate. Although the transport physics of the pulsed plasma is interesting from the viewpoint of momentum loss during the transport, the flow velocity of the pulsed plasma is difficult to define from the waveforms and is not discussed here.

Figure 6(c) shows that I_{target} is increased by the pulsed plasma. As stated in Section 2.3, the increment in I_{target} after triggering the pulse represents the total particle flux by the pulse. A quantitative evaluation of the particle load on the target plate is discussed in Section 3.3. Figure 6(d) shows the V_f values measured using the Langmuir probe. The measured V_f decreases owing

to the pulse, probably because of the higher T_e, induced by ohmic heating after triggering the pulse [16, 17]. The decrease in V_f occurs earlier than the increase in I_{sat}, while both V_f and I_{sat} are measured at the same axial position. The precursor electrons generated in the plasma source may have been present and are observed before the attainment of the ion flux at the Langmuir probe position. Such high-energy electrons are also observed at the beginning of the ELM and discussed in JET [26].

3.3. The particle loads into the Langmuir probe and target plate during the pulse

In this section, we consider the time-integrated particle flux, to investigate the impact of the pulse on the particle load. Regarding the Langmuir probe, the integration of I_{sat} in the time domain has the unit of the fluence. On the other hand, the integrated I_{target} gives the total number of ions in a pulse. The fluence measured by the Langmuir probe and the total number of ions in the target plate are defined by F_{ion} and N_{ion} as follows:

$$F_{\mathrm{ion}} = \frac{1}{eS}\int \left(I_{\mathrm{sat}} - I_{\mathrm{sat\_dc}}\right) \mathrm{d}t, \quad (1)$$

$$N_{\mathrm{ion}} = \frac{1}{e}\int \left(I_{\mathrm{target}} - I_{\mathrm{target\_dc}}\right) \mathrm{d}t, \quad (2)$$

where I_{sat_dc} and I_{target_dc} are the DC components of I_{sat} and I_{target} before the pulse, S is the probe-collecting area, and e is the elementary charge. The particle loads of ions into the probe and the target plate are calculated by time-integrating the ion currents subtracted by the DC components. What F_{ion} and N_{ion} mean are additional flow and ion density during the pulse. The integration interval ranges from 0 to 2 ms.

Figure 7 shows the p_n dependences of F_{ion} and N_{ion}. F_{ion} at the probe position does not strongly depend on p_n and decreases slightly with increasing p_n. The slight reduction in F_{ion} indicates the mitigation of the pulsed plasma by the EIR processes caused by plasma-neutral interactions in the high p_n cases. On the other hand, N_{ion} does not monotonically decrease and exhibits a peak value at p_n ~ 3.0 Pa. The decrease in N_{ion} when p_n is higher than 3.0 Pa might be due to degradation of the pulsed plasma by the EIR processes, as well as F_{ion}. In contrast, N_{ion} decreases with a drop in p_n when p_n is lower than 3.0 Pa. The general tendencies of the particle loads are different at the two positions, with a distance of 200 mm between the Langmuir probe and the target plate. The reason the time-integrated I_{target} decreases under low p_n conditions is explained by showing the time traces in Section 3.4.

3.4. Waveforms of I_{sat} and I_{target} during the pulse

Figure 8 shows the time evolutions of P_{src}, I_{sat}, and I_{target} in various p_n conditions. The

results were averaged over four waveforms, conducted under the same experimental conditions. The low and high p_n cases are separately shown on the left and right sides, respectively. The definition to separate low and high p_n cases is the difference of the I_{target} behavior during the pulse. Figures 8 (a)-(c) show the waveforms when p_n was lower than 3.0 Pa. The lowest p_n value in the present study was 0.44 Pa. However, due to significant heat load to the probe head, I_{sat} could not be acquired during the pulse at p_n of 0.44 Pa and is not shown in figure 8. The time width of the pulsed plasma should be ~ 0.8 ms, as overlapping P_{src} waveforms, as shown in figure 8(a). Figure 8(b) shows I_{sat} with a similar duration at the Langmuir probe position. However, as shown in figure 8(c), the particle flux was not maintained for ~ 0.8 ms at the target plate. The waveforms of I_{target} indicate that the pulse duration detected at the target decreased with a drop in p_n. Because the first parts of the pulsed plasma were detected, their last ones were considered to be partially suppressed in front of the target plate. The suppression mechanism is discussed in detail in Section 4. The reduction in N_{ion}, as decreasing p_n in figure 7(b), was attributed to the suppression of the last parts of the pulsed plasma and to the tendency that the duration of the pulse waveform at the target became shorter with decreasing p_n.

In high p_n cases, on the other hand, I_{sat} and I_{target} in all cases were maintained at least for ~ 0.8, ms as shown in Figures 8(e) and (f). The waveforms of I_{target} were mitigated by increasing p_n. It should be noted that the degradation of pulse duration at the target was not observed when $p_n > 3.0$ Pa and only observed in low p_n cases when $p_n < 3.0$ Pa. The particle loads were lower in both the low and high p_n cases than in the middle p_n case (~ 3.0 Pa). The mechanisms by which the particle flux due to the pulse deceased should be different between low and high p_n cases and are separately described in Section 4.

4. Discussion

4.1. Pulse mitigation under low p_n conditions

Based on the experimental observations that the first part of the pulsed plasma was detected and that the suppression occurred only in the last part of the waveform in low p_n cases, the influence of recycling particles generated by the first part of the pulsed ion flux to the target should be a necessary consideration. To discuss the mitigation mechanism of the pulse, a previous study on power deposition by transient plasma should be covered. A fast infrared camera coupled to a finite element analysis was used to acquire the heat flux deposited by the pulsed plasma inputs on the Magnum-PSI target in Ref. [15]. Clear energy loss was observed in the pulsed plasma with high n_e and the possible interpretations are as follows: Owing to the enhanced recycling of particles in high n_e cases, T_e decreases due to ionization in front of the target. Then, CX collision, which is dominant in low T_e cases, dissipates the pulse energy,

resulting in heat flux reduction. These previous observations are similar to those of the present study. However, it should be noted that there is a difference between the heat and particle fluxes. The heat flux reduction can be explained by the energy dissipation. However, the energy dissipation cannot thoroughly explain the reduction in I_{target}, observed in the present study. Particle flux reduction suggests the existence of a particle sink between the probe and target positions. The physical mechanism by which the particle load owing to the last part of the pulsed plasma is suppressed under low p_n conditions is discussed in the following sections.

4.1.1. Effects of static pressure enhancement

Recycled neutral particles produced by the first part of the pulsed ion flux contributed to an increase in the local p_n in front of the target plate, resulting in a reduction of the last part of the pulsed ion flux by a localized enhancement of plasma detachment. However, this consideration regarding static neutral pressure cannot be exclusive to low p_n cases. The recycling neutral flux should be equal to I_{target} under the present condition, where the singly charged He ions are assumed to be dominant. Figure 8(f) shows a significant I_{target} increment observed in the high p_n cases. For example at p_n of 3.0 Pa, I_{target} is ~ 60 A, which is a comparable level with the I_{target} at p_n of 1.8 Pa in figure 8(c). Although the peak value of I_{target} was similar (~ 60 A) in both cases with p_n of 1.8 and 3.0 Pa, suppression of the last part of the pulsed plasma was observed only at p_n of 1.8 Pa. Hence, the enhancement of the static pressure owing to the recycling process is not sufficient to explain the present results.

4.1.2. Kinetic effects of recycled neutral flow

The kinetic effects of the recycled neutral flow are discussed in this section. Figure 9 shows a schematic illustration. When the pulsed plasma reached the target plate, the ions in the first part of the pulse were accelerated toward the target plate by a potential falling through the sheath. Reflected neutral particles with kinetic energy determined by the sheath potential and energy reflection coefficient were produced as a transient neutral flux in a counter direction to the pulse. Collisions between reflected neutral particles and ions could contribute to momentum and energy reductions in the last part of the pulse. The expected collisions were n-i elastic and CX collisions. In addition to the reactions of recycled neutral particles with the pulsed ions, reactions with background neutral particles should be considered. Once the recycled neutral particles were scattered by the n-n elastic collision, the momentum loss of the pulse plasma cound not be sufficiently obtained. Qualitatively, the n-n collision became dominant over the

n-i collision by increasing p_n. A qualitative consideration of the dominant process under the present experimental conditions is necessary.

Figures 10(a) and (b) show the mean-free paths of CX, $\lambda_{n\text{-}i\_CX}$, and n-i elastic scattering, $\lambda_{n\text{-}i\_EL}$, as functions of the relative kinetic energy of a recycled neutral particle and target ions, $E_{n\text{-}i}$, and the ion density, n_i. On the other hand, figure 10(c) shows the mean-free path of n-n elastic scattering, $\lambda_{n\text{-}n\_EL}$, as the functions of the relative kinetic energy of a recycled neutral particle and target background neutral particles, $E_{n\text{-}n}$, and p_n. The cross-sections of the n-i and n-n collisions are defined as momentum transfer cross-sections [27, 28]. For the calculation, Maxwellian distribution was used for the target ions in figures 10(a) and (b), with an ion temperature, T_i, of 4 eV. Because the Coulomb collision time between ions in pulsed plasma was fairly shorter than the transport time of the pulse from source to target, the Maxwellian distribution was assumed for the target ions. The target background neutral particles in figure 10(c) were assumed to have a temperature of 300 K. Both $\lambda_{n\text{-}i\_CX}$ and $\lambda_{n\text{-}i\_EL}$ decreased with increasing n_i, indicating that the collisions of recycled neutral particles with ions were enhanced in high-density cases such as pulsed plasma. According to the pulsed plasma parameter in Magnum-PSI [14], n_i was expected to be lower than 10^{21} m^{-3} because of the low B in the present study. The relative energy could be determined from the potential fall through the sheath and the energy reflection coefficient. The former might be roughly estimated to be ~45 eV by the potential difference between the plasma potential of -15 V, measured by the Langmuir probe under steady-state conditions [19] and a target bias voltage of -60 V. The latter was ~ 0.43 in the case of He with an incident energy of 45 eV at normal incidence into W [29]. Because of the ambiguity of the plasma potential during the pulses, $E_{n\text{-}i}$ and $E_{n\text{-}n}$ were assumed to be in the range of 10-40 eV in the present experiments. Based on the above assumption shown by the black boxes in figures 10 (a) and (b), $\lambda_{n\text{-}i\_CX}$ and $\lambda_{n\text{-}i\_EL}$ were expected to be ~ 0.03 m and ~0.1-0.3 m, respectively. Because of the small cross-section of the n-i elastic collision in the high $E_{n\text{-}i}$ range, $\lambda_{n\text{-}i\_EL}$ was considered to be larger than $\lambda_{n\text{-}i\_CX}$, implying that the CX process was dominant in determining momentum loss. However, the momentum loss could not completely explain the current drop at the target, as discussed in Section 4.1.3. On the other hand, $\lambda_{n\text{-}n\_EL}$ expected for low p_n and high p_n cases are shown by black boxes in figure 10(c). $\lambda_{n\text{-}n\_EL}$ at low p_n is ~0.1 m and the relation of $\lambda_{n\text{-}i\_CX} < \lambda_{n\text{-}n\_EL}$ indicates that the CX of recycled neutral particles with pulse ions was more dominant than elastic scattering with background neutral particles. Pulse suppression could be caused by enhanced n-i collisions in the low p_n cases. Furthermore,

the tendency was more significant when p_n decreased because $\lambda_{n\text{-}n\_EL}$ increased. The timescale of the interaction between the recycled neutral flux and the pulsed ions, estimated as a CX collision time of ~ 1 μs, is smaller than the decay time of I_{target} (~ 0.1 ms) for low p_n cases, as shown in figure 8(c). Also from this perspective, n-i collision should be a possible reason for affecting the suppression of I_{target}. Conversely, the $\lambda_{n\text{-}n\_EL}$ decreased as p_n increased. $\lambda_{n\text{-}n\_EL}$ was comparable to the $\lambda_{n\text{-}i\_CX}$ at p_n > 3.0 Pa. The relation $\lambda_{n\text{-}i\_CX} \geqq \lambda_{n\text{-}n\_EL}$ indicated a lower contribution of recycled particles to the pulse mitigation. These tendencies are reasonable to qualitatively explain the experimental results. The CX process of recycling particles with the ions after the input of the first part of the pulsed plasma could be essential to suppress the last part of the pulsed plasma in low p_n cases.

4.1.3. Simple modeling of the interaction between pulsed plasma and recycled neutral flux

A possible reason that partial suppression of the pulsed ion flux was exclusive to low p_n cases and not observed in high p_n cases was discussed in the previous paragraph. Next, the dynamic neutral pressure due to the recycled neutral flux to suppress pulsed plasma propagation is discussed. To investigate the neutral particle behavior, modeling was conducted using a fluid code LINDA (LINear Divertor Analysis) [30] coupled with a neutral transport code [31, 32]. The LINDA code is a two-dimensional (2D) plasma fluid code for linear plasma devices. The LINDA code was used to assess the cooling efficiencies of various gas species in the GAMMA 10/PDX [33] and to study the particle, momentum and energy source terms, based on the rate coefficients with the collisional-radiative (CR) code in NAGDIS-II [34]. The neutral transport code is a three-dimensional (3D) Monte-Carlo simulation code for tracing neutral particles introduced into a vacuum vessel until they are ionized or evacuated. The modeling procedure was as follows: First, the plasma distribution was calculated using the LIDNA code to reproduce the pulsed plasma condition without the neutral particles. Boundary conditions at the source side with $T_e = 4$ eV, $T_i = 4$ eV, and $n_e = 10^{20}$ m^{-3} were employed. The energy transmission factors at the target plate were assumed as 2.5 for both ions and electrons. Other calculation setups, such as the Bohm criterion at the target plate and the mesh structure, were similar to those in a previous study [34]. Here, the homogeneous plasma profile from the plasma source to the target in an axial position, Z, was calculated as a steady-state condition. Therefore, this calculation condition simulated the situation just before the pulsed plasma reached the target under quite a low p_n condition. Second, the neutral transport code traced the neutral particles

released from the target surface with a constant energy of ~30 eV in the normal direction and with a particle flux of 1.4×10^{24} $m^{-2}s^{-1}$. To clarify the effects of the recycled neutral particles immediately after the pulsed plasma reached the target, the pump coefficients at all walls were defined as 1.0, so that the thermalized neutral particles were eliminated. Further, the background neutral particles were not simulated, to estimate the momentum loss only due to the recycled neutral flux.

Figure 11 shows the parameter profiles as a result of the neutral transport code where the target plasma was given by the LINDA simulation: (a) neutral He density, n_{He}, and momentum sources for (b) elastic collision, $S_{\mathrm{mu\_EL}}$, and (c) CX, $S_{\mathrm{mu\_CX}}$. The length of the calculation is 2.05 m along the magnetic field line from the anode position at Z = 0 m to the target Z = 2.05 m. Note that the machine length is not consistent with Magnum-PSI because the calculation mesh in the previous study [34] was used. The difference in the machine length had an insignificant effect on the results because the impacts of the recycled neutral flux were localized in front of the target. As shown in figure 11(a), He atoms are localized in front of the target, indicating that strong scattering by high-density ions occurs. The negative values in figures 11(b) and (c) represent the momentum losses. The CX plays a significant role as a momentum sink rather than an elastic collision. The relation $S_{\mathrm{mu\_CX}} < S_{\mathrm{mu\_EL}}$ should be due to $\lambda_{\mathrm{n\text{-}i\_CX}}$ being shorter than $\lambda_{\mathrm{n\text{-}i\_EL}}$ under present conditions.

The dynamic pressure of the recycled neutral flux, which impacts on the plasma, is calculated from the momentum loss and compared with the pulsed plasma pressure. The one-dimensional (1D) plasma momentum conservation can be described as follows [35]:

$$\frac{\mathrm{d}}{\mathrm{d}z}(m_{\mathrm{i}} n_{\mathrm{i}} v^2 + p_{\mathrm{i}} + p_{\mathrm{e}}) = S_{\mathrm{mu}}, \quad (3)$$

where m_{i} is the mass of the ion, v is the ion flow velocity parallel to the magnetic field line, and p_{i} and p_{e} are the static ion and electron pressures, respectively. The terms for transient and viscosity effects, which are included in the conventional fluid equation, are not considered in the present study. The source term, S_{mu}, is expressed as:

$$S_{\mathrm{mu}} = S_{\mathrm{mu\_EL}} + S_{\mathrm{mu\_CX}}. \quad (4)$$

Here, to focus on the momentum sink by n-i collisions (elastic and CX), the momentum source by e-n ionization and the sink by EIR processes were neglected. According to eq. (3), the gradient of the total pressure was the momentum source. Therefore, the integrated momentum sink along the axial position corresponded to the pressure induced by the recycled neutral flux,

which pressed the pulsed plasma in a counter (upstream) direction. When the pressure of the recycled neutral flux was larger than the total pressure of the pulsed plasma, the target current should have been attenuated because of the suppression of the transport and accumulation of the pulsed plasma. The counter pressure of the CX of the recycled neutral particles was calculated to be ~ 6 kPa by the integration of S_{mu_CX}, as shown in figure 11(c), in the Z direction.In contrast, the total pressure of the pulsed plasma was ~ 300 Pa, which was calculated from the summation of the dynamic pressure and static pressure with T_e = 4 eV, T_i = 4 eV, and $n_e = 10^{20}$ m^{-3}. The momentum loss due to the recycled neutral flux was sufficient to compensate for the total pressure of the pulsed plasma from upstream. As discussed above, the enhancement of the recycling might have induced a dynamic pressure by the transient neutral flux and prevented the pulsed plasma from reaching the target plate.

The pulsed plasma pressure could be balanced by the dynamic pressure due to the recycled particles. However, the force exerted by the recycled neutral flux to press the pulsed plasma was insufficient to completely illustrate the reduction in I_{target}. This was because the I_{target} was the particle flux. Even with the strong momentum loss due to the CX process in front of the target, the particle balance was conserved without the particle source or sink. There must have been the particle loss processes, such as radial transport enhanced by the pulsed plasma injection or strong EIR processes due to energy loss by the recycled neutral flux. The former could be observed by particle diagnostics using Langmuir probes located far from the plasma column. The latter could be modeled by an advanced code, which would take into account the dynamic effects, including the transient plasma response.

The ion bombardment results in the secondary electron emission, and subsequent ionization could increase the ion density in front of the target. The secondary electron emission yield for He ion impact at 45 eV on W surface is ~ 0.27 [36]. Such an effect by the secondary electron emission could enhance the interaction between recycled neutral flux and pulsed plasma, however is not discussed in the present study.

4.2. Pulse mitigation under high p_n conditions

The present experiments performed in the high p_n cases seem to demonstrate heat pulse mitigation with a completely different mechanism from the present low p_n cases and Ref. [15]. Recycled neutral particles have difficulty interacting with pulsed plasma because the collisions of recycled particles with background neutral particles are comparable to the collisions with pulsed ions in high p_n cases, as discussed in Section 4.1.2. Therefore, the waveforms of I_{target},

which are mitigated by increasing p_n in figure 8(f), should be affected by the interaction between the pulsed plasma and the background neutral particles before the pulse attains the target plate. The reduction is attributed to the enhanced EIR processes in the pulsed plasma, due to a decrease in T_e. The reduction in T_e should be accompanied by an energy loss of ions by CX and the electron-ion energy relaxation process dominant in a high-density case [37]. To confirm the enhanced EIR processes, the investigation of T_e and OES for detecting highly excited atoms during the pulse should be investigated in the future. We note that the present experimental observations in high p_n cases indicate the effectiveness of plasma detachment for pulsed plasma mitigation by enhanced plasma-neutral interactions.

5. Conclusions

To study the impacts of the transient enhancement of recycling on the target ion flux into the detached divertor, fundamental experiments regarding the neutral pressure, p_n, dependence of the particle load with pulsed plasma input were performed in the linear plasma device Magnum-PSI. Transient phenomena during the pulsed plasma were measured using a reciprocating Langmuir probe and the target plate. The floating potential of the Langmuir probe indicated the presence of precursor electrons after triggering the pulse. The time-integrated target current exhibited a peak value at p_n of 3.0 Pa, whereas the integrated particle flux by the Langmuir probe monotonically decreased as p_n increased. Suppression of the last part of the particle flux was observed at the target plate in low p_n cases. In contrast, the target flux was mitigated in high p_n cases because of the interaction of the pulsed plasma with the background neutral particles, indicating the effectiveness of plasma detachment in pulsed load mitigation. Regarding the low p_n cases, because the mean-free path of the charge exchange was shorter than that of the n-n elastic scattering, the impact of the recycled neutral flux on the pulsed plasma suppression by the transient enhancement of the plasma-neutral interaction was speculated. Modeling was performed by coupling the LINDA code with a neutral transport code. The modeling results showed that the dynamic pressure induced by the transient recycled neutral flux in the opposite direction from the target caused a sufficient momentum loss to stagnate the pulsed plasma.

The suppression mechanism is discussed with respect to the pulse condition. In steady-state plasma, a similar reduction in the steady-state heat load cannot be expected. This is because the collision of recycled neutral particles with background ones is much more dominant, in most cases, in linear plasma devices. To reproduce the recycling neutral flux to suppress the steady-state heat load, an experimental condition with a high density and low p_n is desired. The impact of recycled neutral flux is highlighted in the present study because the experiments were

performed under a fairly high-density condition with a transient pulse in Magnum-PSI.

The discussion, including recycling, could indicate that a low p_n operation has the possibility of suppressing the ELM as well as a high p_n condition. When future fusion devices operate in a middle p_n regime in the divertor region, a significant transient heat load owing to the ELM input can be considered. Further studies regarding the recycling of particles from the viewpoint of energy-loss processes are necessary to explain the present experimental observations in detail. Additional experiments on heat flux measurements under pulse plasma conditions will also be useful for discussing the impact of the recycled neutral flux on the kinetic energy of pulsed plasma.

Data availability statement

Raw data were generated at the Magnum-PSI facility. Derived data supporting the findings of this study are available from the corresponding author upon reasonable request.

Acknowledgments

We greatly appreciate the Magnum-PSI team for their technical support with the experiments. This work was supported by JSPS KAKENHI Grant Numbers JP17KK0132, JP18KK0410, JP19K14686, JP20H00138, JP21KK0048, and JP22H01203 and NIFS/NINS under the Young Researchers Supporting Program. The Magnum-PSI facility at DIFFER was funded by the Netherlands Organization for Scientific Research (NWO) and EURATOM. DIFFER is part of the institute's organization of NWO and a partner in the Trilateral Euregio Cluster TEC.

References

[1] Pitts R.A., Andrew P., Arnoux G., Eich T., Fundamenski W., Huber A., Silva C., Tskhakaya D. and JET EFDA Contributors 2007 *Nucl. Fusion* **47** 1437

[2] Loarte A. *et al* 2014 *Nucl. Fusion* **54** 033007

[3] Leonard A.W. 2018 *Plasma Phys. Control. Fusion* **60** 044001

[4] Ohno N. 2017 *Plasma Phys. Control. Fusion* **59** 034007

[5] Loarte A. *et al* 2007 *Nucl. Fusion* **47** S203

[6] Field A.R. *et al* 2017 *Plasma Phys. Control. Fusion* **59** 095003

[7] Wischmeier M., Kallenbach A., Chankin A.V., Coster D.P., Eich T., Herrmann A., Müller H.W. and ASDEX Upgrade Team 2007 *J. Nucl. Mater.* **363**–**365** 448

[8] F.M. Laggner *et al* 2018 *Plasma Phys. Control. Fusion* **60** 025002

[9] Brezinsek S. *et al* 2016 Phys. Scr. **T167** 014076

[10] Ohno N., Tanaka M., Ezumi N., Nishijima D., Takamura S., Krasheninnikov S.I., Pigarov A.Yu. and Park J. 1999 *Phys. Plasmas* **6** 2486

[11] Ohno N. *et al* 2001 *Nucl. Fusion* **41** 1055

[12] Scholten J. *et al* 2013 *Fusion Eng. Des.* **88** 1785

[13] van Eck H.J.N. *et al* 2019 *Fusion Eng. Des.* **142** 26

[14] Li Y. *et al* 2021 *Plasma Phys. Control. Fusion* **63** 085016

[15] van Eck H.J.N. *et al* 2014 *Fusion Eng. Des.* **89** 2150

[16] Zielinski J.J. T.W. van der Meiden H.J., Morgan T.W., Schram D.C. and Temmerman G.D. 2012 Plasma Sources Sci. Techno. **21** 065003

[17] Morgan T.W., de Kruif T.M., van der Meiden H.J., van den Berg M.A., Scholten J., Melissen W., Krijger B.J.M., Bardin S. and Temmerman G.D. 2014 Plasma Phys. Control. Fusion **56** 095004

[18] Hayashi Y., Ohno N., van der Meiden H.J., Scholten J., Kajita S., van den Berg J., Perillo R., Vernimmen J. and Morgan T.W. 2019 *Plasma Fusion Res.* **14** 1202135

[19] Tanaka H. *et al* 2020 *Plasma Phys. Control. Fusion* **62** 115021

[20] van den Berg M.A., Brons S., Kruijt O.G., Scholten J., Pasquet R., Smeets P.H.M., Schweer B. and Temmerman G.D. 2011 *Fusion Eng. Des.* **86** 1745

[21] van der Meiden H.J. *et al* 2012 *Rev. Sci. Instrum.* **83** 123505

[22] Nishijima D., Wenzel U., Motoyama M., Ohno N., Takamura S. and Krasheninnikov S.I. 2001 *J. Nucl. Mater.* **290**–**293** 688

[23] Ohno N., Ezumi N., Nishijima D. and Takamura S. 1998 *Czech. J. Phys.* **48** 127.

[24] Krasheninnikov S.I., Rensink M., Rognlien T.D., Kukushkin A.S. Goetz J.A., LaBombard B., Lipschultz B., Terry J.L. and Umansky M. 1999 *J. Nucl. Mater.* **266**-**269** 251.

[25] Krasheninnikov S.I., Kukushkin A.S., Lee Wonjae, Phsenov A.A., Smirnov R.D., Smolyakov A.I., Stepanenko A.A. and Zhang Yanzeng 2017 *Nucl. Fusion* **57** 102010.

[26] Guillemaut C. *et al.*, 2018 *Nucl. Fusion* **58** 066006

[27] Rychlewski J. (Ed.) E*xplicitly Correlated Wave Functions in Chemistry and Physics: Theory and Applications* (Progress in Theoretical Chemistry and Physics (13)) (Springer; Softcover reprint of the original 1st ed. 2003 ver. (2010/12/4))

[28] Bachmann P. and Reiter D. 1995 *Contrib. Plasma Phy.* **35** 45

[29] Eckstein W. "Reflection (Backscattering)", *IPP Report 17/12 Max-Planck Institut fuer Plasmaphysik*, August 2009

[30] Furuta T., Takeda H., Toma M., Sato W., Homma Y., Sawada Y., Nakashima Y., and Hatayama A. 2013 *Fusion Sci. Technol.* **63** 411

[31] Goto M., Sawada K., Fujii K., Hasuo K. and Morita S. 2011 *Nucl. Fusion* **51** 023005

[32] Sawada K., Nakamura H., Kobayashi M., Haga K., and Hasuo M. 2020 *Contrib. Plasma Phys.* **60** e201900153

[33] Islam M.S., Nakashima .Y and Hatayama A. 2017 *Plasma Phys. Control. Fusion* **59** 125010

[34] Tanaka H., Saeki I., Ohno N., Kajita S., Ido T., Natsume H., Hatayama A., Hoshino K., Sawada K., and Goto M. 2020 *Phys. Plasmas* **27** 102505

[35] Stangeby P.C. "The Plasma Boundary of Magnetic Fusion Devices", *Institute of Physics Publishing*, London, 2000

[36] Czack G. and Kirschstein G. 1993 Gmelin Handbook of Inorganic and Organometallic Chemistry (W Supplement vol A4) 8th edn (Berlin: Springer).

[37] Hayashi Y., Ješko K., van der Meiden H.J., Vernimmen J.W.M., Morgan T.W., Ohno N., Kajita S., Yoshikawa M. and Masuzaki S. 2016 *Nucl. Fusion* **56** 126006

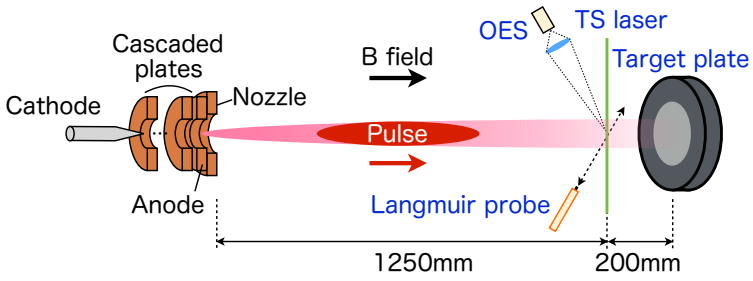

Figure. 1: A schematic of the experimental setup in Magnum-PSI. Positions of diagnostics (Langmuir probe, target plate, TS, and OES) are depicted. (Single column)

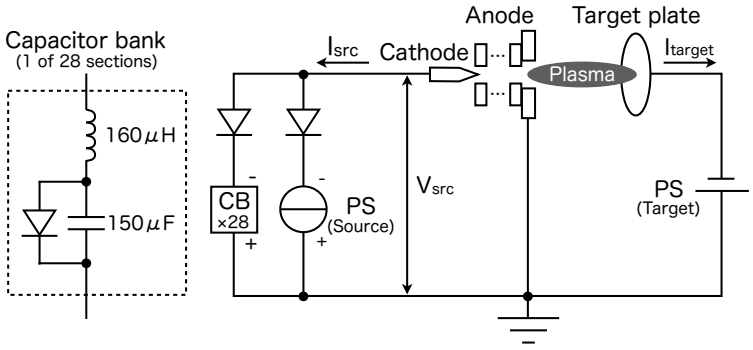

Figure. 2: Discharge circuit for compatible operation of steady-state DC discharge and transient pulse. The target plate is negatively biased for collecting the ion current. (Single column)

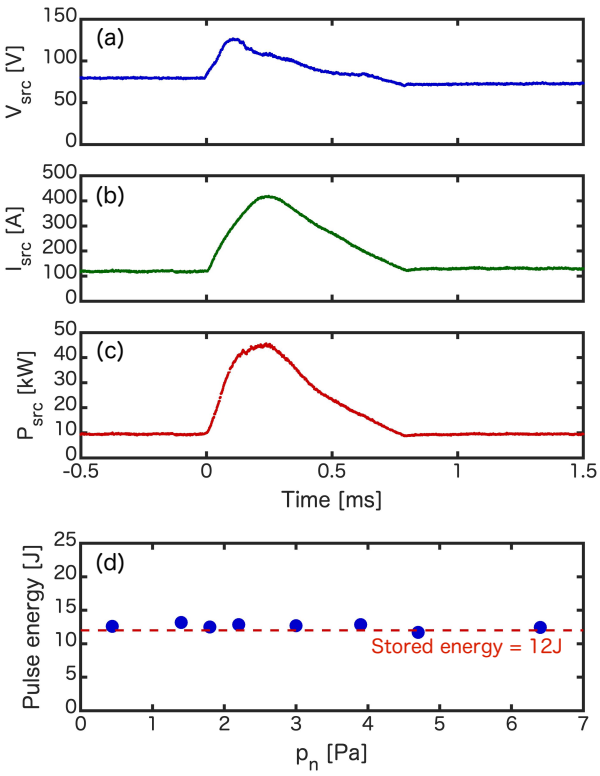

Figure. 3: Time traces of (a) V_{src}, (b) I_{src}, and (c) P_{src} during a pulse at p_n of 3.0 Pa. The trigger timing of the pulse is defined as $t = 0$ s. (d) p_n dependence of the dissipated pulse energy in the source plasma is calculated by the time-integration of the AC component of P_{src}. (Single column)

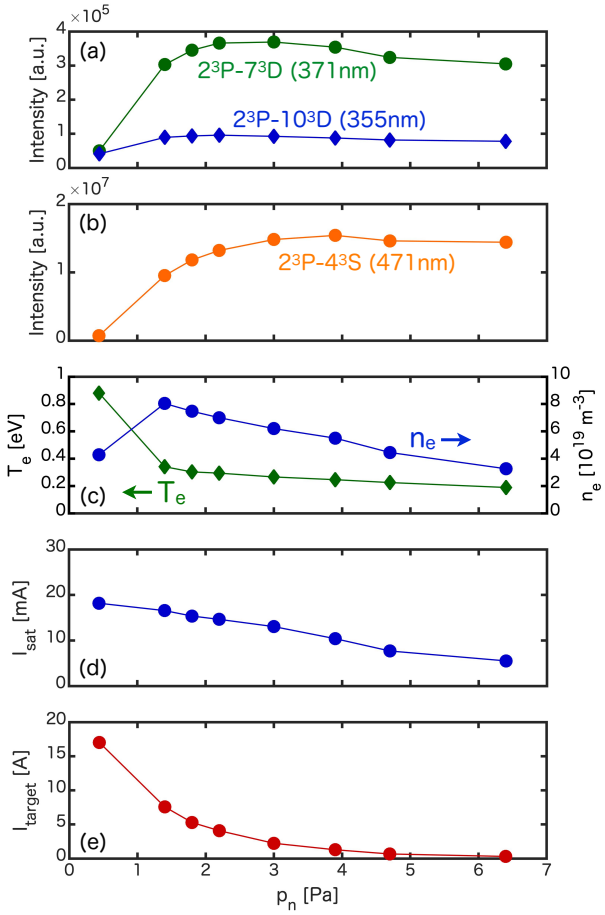

Figure. 4: p_n dependences of the emission intensities of the transitions from (a) high-n states (370.5 nm: 2^3P-7^3D and 355.4 nm: 2^3P-10^3D) and (b) low-n state (471.3 nm: 2^3P-4^3S), (c) n_e and T_e by TS measurement, (d) I_{sat} at the Langmuir probe and (e) I_{target} at the target plate. (Single column)

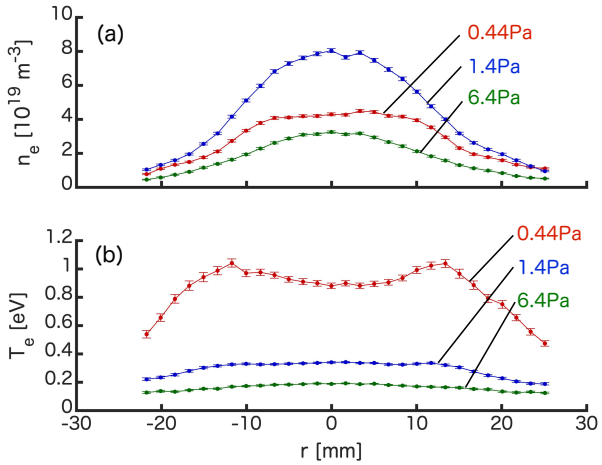

Figure 5: Radial profiles of (a) n_e and (b) T_e by TS measurement at various p_n of 0.44, 1.4, and 6.4 Pa. (Single column)

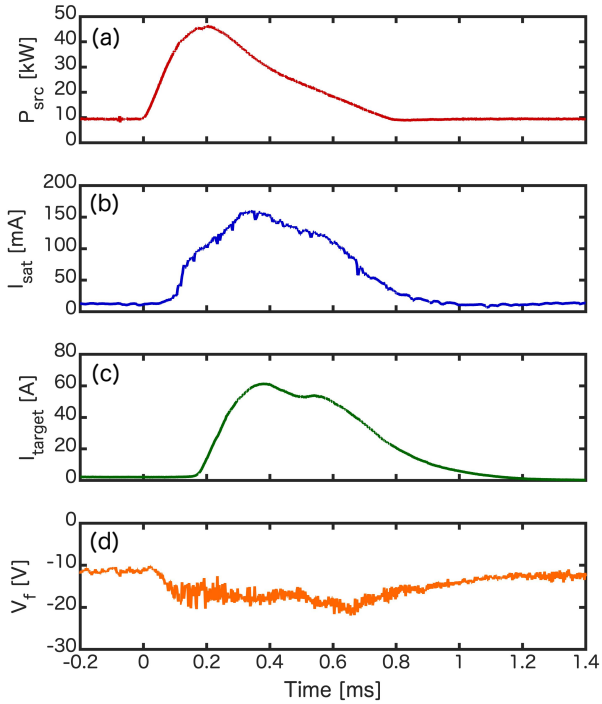

Figure 6: Temporal evolutions of (a) P_{src}, (b) I_{sat}, (c) I_{target} and (d) V_f during the pulse at p_n of 3.0 Pa. Four waveforms conducted under the same condition were averaged for the plot. (Single column)

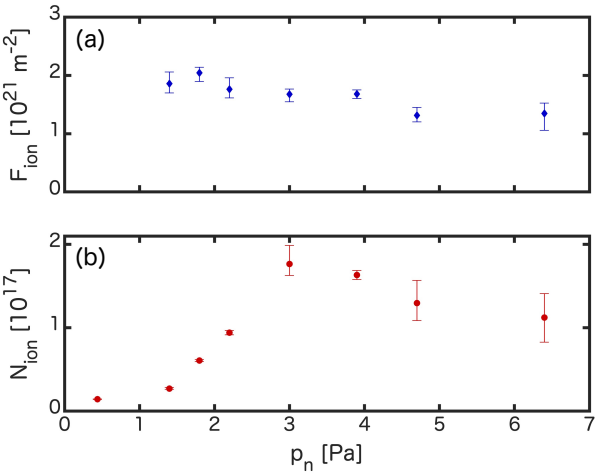

Figure 7: p_n dependences of (a) F_{ion} and (b) N_{ion}. An error bar represents the maximum and minimum values in four data acquisition at each p_n condition. Because of the significant heat load into the probe head, F_{ion} could not be obtained at p_n of 0.44 Pa. (Single column)

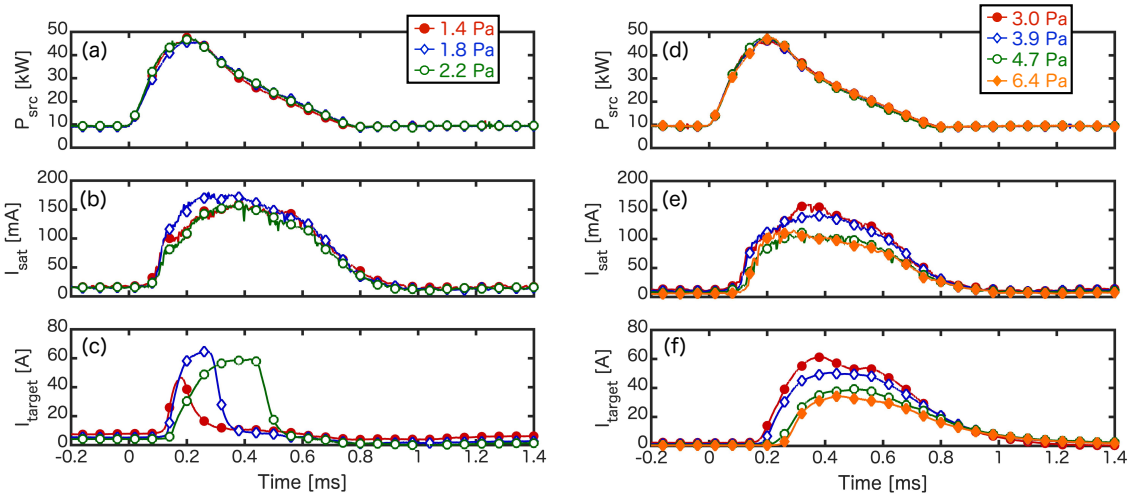

Figure 8: Time traces of (a) and (d) P_{src}, (b) and (e) I_{sat}, and (c) and (f) I_{target} during the pulse. Low and high p_n cases are separately shown on left- and right-hand side, respectively. Four waveforms conducted under the same experimental conditions were averaged for the plot. (Double column)

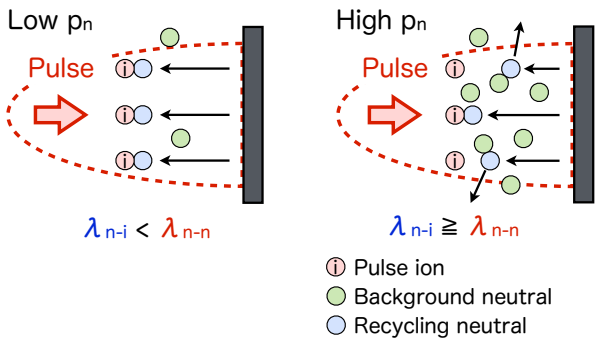

Figure 9: Schematic illustration of the impacts of recycled neutral particles on the last part of the pulsed plasma in low and high p_n cases. (Single column)

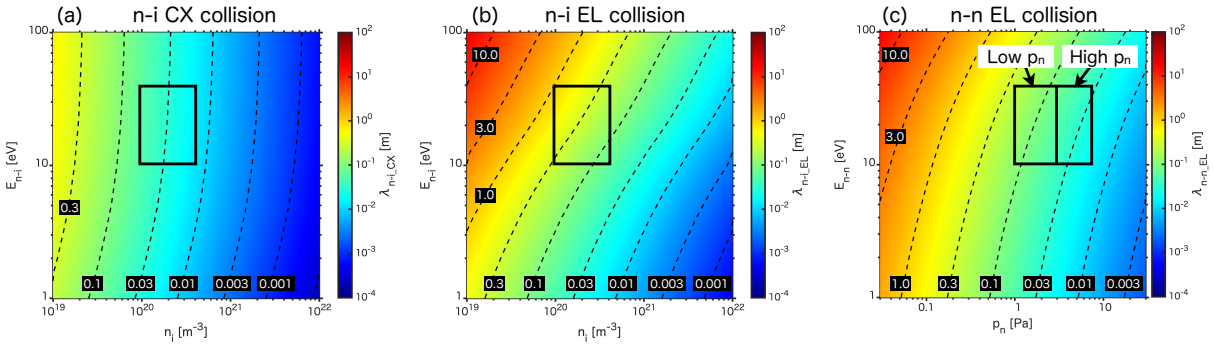

Figure 10: (a) $\lambda_{n\text{-}i\_CX}$ and (b) $\lambda_{n\text{-}i\_EL}$ plotted as the functions of $E_{n\text{-}i}$ and n_i. (b) $\lambda_{n\text{-}n\_EL}$ plotted as the functions of $E_{n\text{-}n}$ and p_n. The Maxwellian distribution was considered for the target ions and the target background neutral particles. T_i and neutral particle temperatures were assumed to be 4 eV and 300 K, respectively. (Double column)

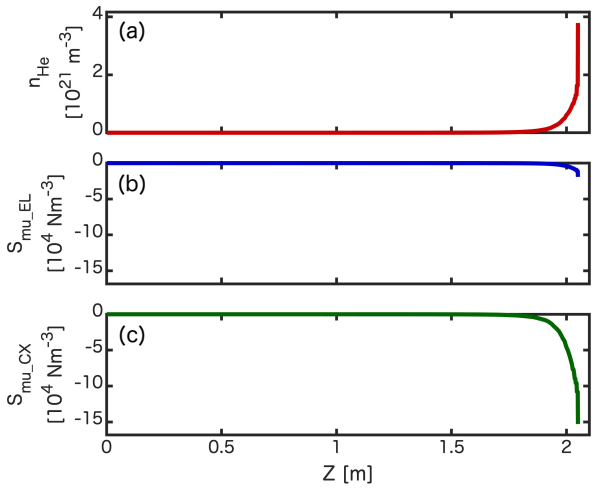

Figure11: Modeling results of (a) n_{He}, (b) $S_{\mathrm{mu\_EL}}$ and (c) $S_{\mathrm{mu\_CX}}$ along the magnetic field line. Axial length is not consistent with Magnum-PSI because the calculation mesh with the previous study [32] was used. (Single column)